

# A Universal Transformer-Based Coarse-Grained Molecular Dynamics Framework for Protein Dynamics

Jinzhen Zhu<sup>1, a)</sup>

Shanghai AI Laboratory, Shanghai, 200030, China

(Dated: 11 February 2025)

We present a novel, universal, Transformer-based coarse-grained molecular dynamics (CG-MD) framework for simulating protein dynamics. Our trained model generalizes to all protein systems, regardless of sequence length or number of chains. First, we extend a tree-structured protein representation to accommodate multi-chain proteins, demonstrating sub-angstrom-level accuracy in reconstructing a 169-amino-acid protein structure. Then, representing collective variables as language-like sequences, we use a Transformer network as a propagator for stochastic differential equations, generating MD trajectories over 10,000 times faster than all-atom MD simulations. This single trained model accurately simulates both single-chain and two-chain proteins, and the generated trajectories closely resemble all-atom MD trajectories in their RMSD profiles. With sufficient training data, we anticipate that our model can achieve universality across all proteins, offering a 10,000x acceleration of MD simulations with high accuracy.

## I. INTRODUCTION

Molecular dynamics (MD) simulations are essential for understanding protein structure and function, playing a crucial role in areas like drug design<sup>1</sup>. However, the computational cost of simulating large biomolecules over relevant timescales remains a significant bottleneck<sup>2</sup>. While hardware advancements, such as GPUs<sup>3</sup> and specialized supercomputers<sup>4</sup>, have provided some relief, software improvements offer complementary solutions. Enhanced sampling techniques<sup>5</sup> and coarse-grained (CG) MD simulations are prominent examples. CG methods, which represent groups of atoms as single interaction centers, offer a compelling balance between accuracy and computational efficiency. However, challenges remain in accurately capturing complex protein motions and solvent effects.

Two primary paradigms, "top-down" and "bottom-up"<sup>6</sup>, guide CG model development. Bottom-up approaches, leveraging statistical mechanics to define effective interactions<sup>7</sup>, have yielded numerous successful CG models for protein dynamics<sup>8–15</sup>. Recently, machine learning (ML) has further enhanced CG simulations, with deep neural networks (DNNs) being used to approximate potential energy surfaces<sup>13,14</sup> and even Transformer models being applied to accelerate MD computations based on atomic coordinates<sup>15</sup>. Despite these advances, a universal and efficient framework for generating protein trajectories, particularly for multi-chain systems, remains an open challenge.

Our previous work<sup>16</sup> introduced a coarse-grained molecular dynamics framework that successfully reconstructed protein dynamics by combining a tree-structured protein representation with AI techniques, including deep neural networks and real-NVP generators, to approximate stochastic differential equations. A key limitation of this approach was its reliance on protein-specific training data and network architectures, hindering its broader applicability.

In this paper, we address this challenge by developing a

more generalizable framework. First, we extend our tree-structured protein representation to handle multi-chain proteins. Second, we introduce a novel data representation that incorporates protein sequence information into the coarse-grained parameters. This generalized representation allows us to leverage the power of Transformer-based models, which are inherently independent of the target protein's size, number of chains, sequence, and specific structural features. We validate our approach by demonstrating accurate reconstruction of the multi-chain protein 3sj9 and by precisely predicting the MD trajectories of two smaller proteins: the two-chain protein 1bom and the single-chain protein 1l2y (including mutants). Training the Transformer model on a diverse dataset of protein trajectories results in a highly accurate and generalizable model. We believe that with sufficient training data, our universal Transformer-based framework has the potential to simulate the dynamics of any protein, regardless of its complexity or sequence.

## II. METHODS

### A. Collective variables

As is shown in our previous work, the local coordinate  $\vec{x}_l$  and global  $\vec{x}_g$  coordinate conversion could be written as

$$\begin{bmatrix} \vec{x}_g \\ 1 \end{bmatrix} = \hat{M}(\vec{\varphi}, \vec{T}) \begin{bmatrix} \vec{x}_l \\ 1 \end{bmatrix}, \quad (1)$$

where the coordinate transformation matrix could be written as

$$\hat{M}(\vec{\varphi}, \vec{T}) = \begin{bmatrix} \hat{R}(\vec{\varphi}) & \vec{T} \\ \vec{0}^T & 1 \end{bmatrix}, \quad (2)$$

where  $\vec{\varphi} = [\varphi_1 \ \varphi_2 \ \varphi_3]^T$  and  $\vec{T} = [O_x \ O_y \ O_z]^T$  are  $3 \times 1$  vectors with each element representing the rotation and translational components. Although only 2 elements of  $\vec{\varphi}$  is sufficient for representing the rotation, a size 3 vector is used for notational convenience. Eq. 1 is universal both for the coordinates transformations between chains and the global protein,

<sup>a)</sup>Electronic mail: zhujinzenlmu@gmail.com

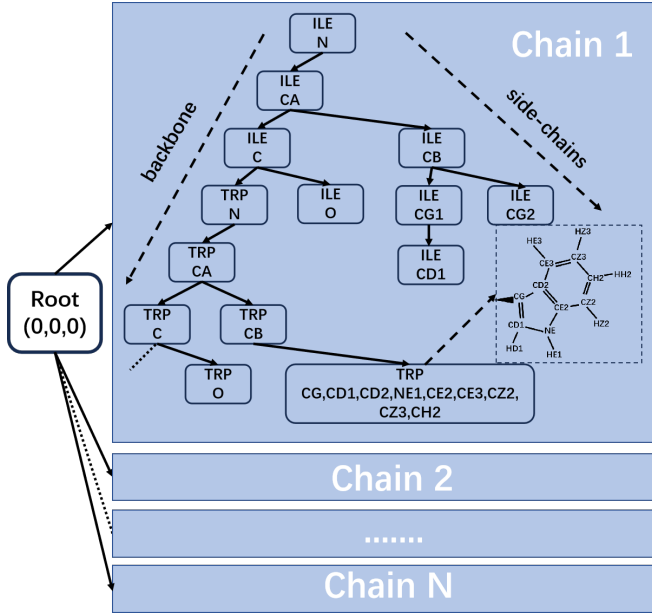


FIG. 1: This illustration depicts coordinate transform (upper) and tree structure of CVs of atoms in proteins (lower) illustration. An artificial protein compound with first two amino acids being ILE and TRP for the first chain is applied to illustrate the tree-structure.

and those among different hierarchies in the tree structure of a chain. The difference lies in the  $\vec{T}$  in Equation 2, which is always fixed for transformations inside a chain. Thus, similar to the tree data structure in chain 1 in Figure 1, the data representation among the chains could also be treated as hierarchies in the tree, where we take an virtual point in the axis as the root. The root node can be arbitrary and the global origin  $(0, 0, 0)$  is selected for convenience, whose children are the roots (first  $N$  atoms) of the chains, illustrated in Figure 1. For details of the tree-structure presentation of proteins, please refer to our previous work.

Transformer-based deep learning frameworks have demonstrated significant success in natural language processing and are increasingly applied in scientific domains, particularly in the development of AI force fields for molecular dynamics, as exemplified reference<sup>15</sup>. A key advantage of the Transformer architecture is its ability to handle variable input sequence lengths, allowing a trained model to adapt to inputs of arbitrary length. By representing protein collective variables as linguistic sequences, we can effectively integrate the Transformer model into our learning process.

We now describe the transformation of collective variables into a language sequence format. Consider a  $C$ -chain protein compound, where  $c$  indexes the chains ( $c = 1, \dots, C$ ). Each chain  $c$  is characterized by its rotational and translational frame vectors, denoted as  $\vec{\varphi}_c$  and  $\vec{T}_c$ , respectively, and has a sequence length  $N_c$ . The collective variable  $S_t$  at time  $t$  is represented as a matrix of dimensions  $[2 + \sum_1^C N_c] \times 2L$ , where  $L$  is a constant. Empirically, we determined that  $2L \approx 40$  represents the minimum tensor dimension required for data storage.

This value,  $2L$ , is subsequently used as the tensor dimension within our model. This data matrix, denoted as

$$S_t = \begin{bmatrix} \vec{T}^T \\ \vec{\theta}_f^T \\ \hat{\theta}_1 \\ \vdots \\ \hat{\theta}_c \\ \vdots \\ \hat{\theta}_C \end{bmatrix}, \quad (3)$$

can be structured as follows: the first row contains the translational coordinates (positions of the first  $N$  atoms in each chain), the second row contains the corresponding rotational angles of the sub-coordinates within each chain, and the subsequent rows contain information specific to each protein chain.

Information for the  $c$ -th chain is encoded in matrices  $\hat{\theta}_c$  and  $\hat{S}_c$ . As established in previous work (cite), only a subset of bond and dihedral angles is required to represent each protein chain. Within  $\hat{\theta}_c$ , the  $i$ -th row stores the dihedral and bond angles,  $\vec{\theta}_i^c$ , of the  $i$ -th amino acid in the sequence. The corresponding row in  $\hat{S}_c$  stores the index and properties of that amino acid, as detailed below

$$\hat{\theta}_c = \begin{bmatrix} \cos \vec{\theta}_1^c & \vec{0}_{L-K_1^c} & \sin \vec{\theta}_1^c & \vec{0}_{L-K_1^c} \\ \vdots & \vdots & \vdots & \vdots \\ \cos \vec{\theta}_i^c & \vec{0}_{L-K_i^c} & \sin \vec{\theta}_i^c & \vec{0}_{L-K_i^c} \\ \vdots & \vdots & \vdots & \vdots \\ \cos \vec{\theta}_{N_c}^c & \vec{0}_{L-K_{N_c}^c} & \sin \vec{\theta}_{N_c}^c & \vec{0}_{L-K_{N_c}^c} \end{bmatrix}, \quad (4)$$

where  $\vec{0}_X^T$  indicates the zero vector with length  $X$ , and serves as a complement to each row. Angles are represented as cosine and sine values to address periodicity.

For consistency across chain blocks, the first two rows, representing the relative positions of each chain, are also transformed into the sine-cosine format. Specifically, the transformation is defined as

$$\vec{T}^T = \begin{bmatrix} \frac{O_x^1}{O_{\max}} & \dots & \frac{O_z^C}{O_{\max}} & \vec{0}_{L-3C} & \sqrt{1 - (\frac{O_x^1}{O_{\max}})^2} & \dots & \sqrt{1 - (\frac{O_z^C}{O_{\max}})^2} & \vec{0}_{L-3C} \end{bmatrix} \quad (5)$$

and

$$\vec{\theta}_f^T = [\cos \varphi_1^1 \dots \cos \varphi_3^C \vec{0}_{L-3C} \sin \varphi_1^1 \dots \sin \varphi_3^C \vec{0}_{L-3C}] \quad (6)$$

where  $O_{\max}$  is a value exceeding any possible coordinate within the simulation box, and  $O_x^c, O_y^c, O_z^c, \varphi_1^c, \varphi_2^c, \varphi_3^c$  represent the origin and rotational angles, respectively, of the  $c$ -th protein chain.

As with most Transformer models, positional encoding is incorporated to capture the position of each amino acid. The positional encoding matrix,  $Pos$ , has the same dimensions as

$S_c$  and is defined as

$$P_{i,j} = \begin{cases} \cos \frac{p(i)+N_{max}c}{f^{(j-1)(pt(i)/100+1)/L}} & \text{if } j \leq L \\ \sin \frac{p(i)+N_{max}c}{f^{(j-1-L)(pt(i)/100+1)/L}} & \text{if } j > L \end{cases}, \quad (7)$$

where  $pt(i)$  returns the amino acid type index (0-19), and  $p(i)$  returns the amino acid index within the chain. For the first two rows (representing frame origins and angles),  $pt(i) = 20$  and  $p(i) = -2$  and  $-1$ , respectively. The factor  $f$  is a user-defined constant typically ranging from 200 to 1000, and  $N_{max}$  represents the maximum possible number of amino acids in a chain. These values are chosen to ensure that the positional encoding uniquely identifies both the position and type of each amino acid. Unlike many language models, our approach includes the amino acid type within the positional encoding. The positional encoding is fixed once the target protein is selected.

The application of positional encoding operator  $\mathbb{P}$  to the coefficient matrix  $S_t$ :  $S_t^P = \mathbb{P}S_t$  goes as

$$S_{i,j}^P = \begin{cases} S_{i,j}P_{i,j} - S_{i,j+L}P_{i,j+L} & \text{if } j \leq L \\ S_{i,j}P_{i,j-L} + S_{i,j-L}P_{i,j} & \text{if } j > L \end{cases}, \quad (8)$$

and the inverse operation:  $S_t = \mathbb{P}^{-1}S_t^P$  is

$$S_{i,j} = \begin{cases} S_{i,j}^P P_{i,j} + S_{i,j+L}^P P_{i,j+L} & \text{if } j \leq L \\ S_{i,j}^P P_{i,j-L} - S_{i,j-L}^P P_{i,j} & \text{if } j > L \end{cases}, \quad (9)$$

where sub-index of  $S_t$  is neglected for notational brevity. Indicating the addition or subtraction of the positional encoding angles in the coefficient matrix.

Concurrently with the positional encoding, a mask matrix,  $M$ , of the same dimensions as the coefficient matrix is constructed.  $M$  contains zeros at the positions corresponding to the zero vectors,  $\vec{0}_X$ , in Equation 3 and ones elsewhere.

## B. Propagation with transformer

### 1. SDE and Propagator

From our previous derivation in Ref CITE, the the propagation of collective variable  $S_{t+i}$ , walking  $i$  steps, from  $t$  time stamp to  $t+i$  time stamp, could be written as

$$S_{t+i} = \overbrace{\mathbb{F}_0 \circ \mathbb{F}_0 \cdots \circ \mathbb{F}_0}^i(S_t) + \mathbb{P}(\boldsymbol{\varepsilon}_{t,i}), \boldsymbol{\varepsilon}_{t,i} \equiv \boldsymbol{\varepsilon}_{t,i}(S(t)) \quad (10)$$

to resemble the stochastic differential equation (SDE). The deterministic operator, which uses  $\mathbb{F}_0$  for one step and  $\overbrace{\mathbb{F}_0 \circ \mathbb{F}_0 \cdots \circ \mathbb{F}_0}^i(S_t)$  for  $i$  steps, is called the drift force. And  $\mathbb{P}(\boldsymbol{\varepsilon}_{t,i})$ , is called the noise term, with  $\boldsymbol{\varepsilon}_{t,i}$  denoting the standard deviation dependent on the CVs at time  $t$  and step size  $i$ .

We have shown in our previous work CITE, that with loss

$$L_{T_n} = \frac{1}{n} \sum_{i=1}^n \frac{1}{T-i} \sum_{t=1}^{T-i} \left\| \mathbf{S}_{t+i} - \overbrace{\mathbb{F} \circ \cdots \circ \mathbb{F}}^i(\mathbf{S}_t) \right\|^2, \quad 1 \leq n \leq T-1, \quad (11)$$

reaches its minimum, the trained network effectively approximates the drift force  $\mathbb{F}_0$  represented in Equation 10. We find the logarithm of  $L_{T_n}$  helps the convergence process during training, thus

$$L_{T_n} = \log \frac{1}{n} \sum_{i=1}^n \frac{1}{T-i} \sum_{t=1}^{T-i} \left\| \mathbf{S}_{t+i} - \overbrace{\mathbb{F} \circ \cdots \circ \mathbb{F}}^i(\mathbf{S}_t) \right\|^2, \quad 1 \leq n \leq T-1, \quad (12)$$

is applied as the loss function in practice.

### 2. Transformer for Propagator

In our previous work, a simple neural network representing the drift force, it proves efficiency and accuracy in reproducing the MD trajectories. However, the size of the neural network depends on the system size of the input protein and the network can only be used for the same system of the training data, making the trained data untransferable to other protein systems.

The new representation of the collective variables in Equation 3, is fixed in the second dimension  $L$ , making it highly applicable for transformer model, which was successfully applied in natural language process (NLP) problem<sup>17</sup> and also in some MD simulations<sup>15</sup>. The  $L$  is the property dimension after embedding operation, and the first dimension  $2 + \sum_1^C N_c$  is the length of a sentence. Making it analogy to the translation problem of the transformer model, the input  $S_t$  is a sentence with  $2 + \sum_1^C N_c$  words, and the translated sentence also has  $2 + \sum_1^C N_c$  words, all the words are embedded to a  $L$  length vector, where the meaning of each word is a property of a single amino acid or the frame property. Note that, we do not need the embedding operations here, as our representation (length  $L$ ) of any amino acid in each row already has its positional property and type property (encoded in  $\hat{S}_c$ , see Equation 3). The structure of a specific amino acid can also be solely defined by  $\hat{\theta}_c$ , see Equation 4. Thus all the information of the protein dynamics could be encoded in the transformer network. The drift force propagator is composed of a sequence of  $N_T$  transformer layers  $\mathbb{T}_i$ , lead by positional encoding operator  $\mathbb{P}$  and followed by combinations of a normalization operator  $\mathbb{N}_\theta$ , inverse positional encoding operator and a masking operator  $\mathbb{M}$ . Before and after the transformer network, two full connected network  $\mathbb{D}_S$  and  $\mathbb{D}_E$  are added. Different from previous We add these two networks as pre and pos process to automatically extract the useful information and then back transform the output the transformer network. Different from the deep learning framework in our previous work, the shape of the two networks are fixed, the input and output dimensions are both  $2L$ . The whole network for the drift force operator goes as

$$\mathbb{F}_0 = \mathbb{M} \circ \mathbb{P}^{-1} \circ \mathbb{N}_\theta \circ \mathbb{D}_E \circ \mathbb{T}_1 \circ \cdots \circ \mathbb{T}_i \circ \cdots \circ \mathbb{T}_{N_T} \circ \mathbb{D}_S \circ \mathbb{P}. \quad (13)$$

The normalization operator normalizes the values sin and cos in each row of  $S_t$ , including the angles of amino acids, frame angles and frame origins, as is shown in Equation 5 and Equation 6, where the origins of each chain are converted to sin

and cos format. The mask first multiplies a predefined matrix with the same shape as  $S_t$ , the matrix elements being the ones except the positions occupied by  $\vec{0}$  in Equation 4, which are all zeros.

While ideally, noise would be directly incorporated into the SDE formulation, this presents challenges in our current implementation. Therefore, to introduce the desired stochasticity during inference, we leverage the dropout mechanism within the Transformer network. Dropout functions as a form of regularization by randomly setting a proportion of neuron outputs to zero during each forward pass. In our context, this random deactivation of neurons effectively simulates the noise component of an SDE, allowing the model to explore a broader distribution of potential trajectories. The dropout rate, controlling the fraction of deactivated neurons, serves as a tunable parameter governing the level of stochasticity introduced.

### 3. Training and model assessment

A key difference from our prior work is the shift from protein-specific DNN models to a unified, Transformer-based architecture. This allows us to train a single coarse-grained model that can be applied to a variety of proteins. The model is trained using a combined dataset of trajectories from multiple proteins, effectively learning a universal representation. We utilize a one-shot training approach, where the model is trained on this diverse dataset and then used for trajectory propagation. During training, an adaptive learning rate strategy is employed, where the learning rate is dynamically reduced based on the loss function’s plateau behavior. Specifically, if the loss does not decrease significantly over several steps, the learning rate is reduced. This fine-tuning method has been found to yield good performance. To further reduce computational cost during training, we apply positional encoding to the entire training dataset prior to training. This allows us to neglect the  $\mathbb{P}$  and  $\mathbb{P}^{-1}$  transformations in Equation 13 during the training process. For model evaluation, a positionally encoded trajectory template is provided as input. Propagation is then performed using Equationation 13 without the  $\mathbb{P}$  and  $\mathbb{P}^{-1}$  transformations. Finally, the Cartesian coordinate trajectory is generated in parallel from the generated collective variable trajectories. This parallel generation process is computationally efficient and amenable to optimization.

For the analysis of the model, a frame of the test trajectory is selected and feed into the model, then the propagator generates a trajectory. We quantify the overall structural similarity between the generated and reference trajectories by calculating the RMSD difference ( $\Delta\text{RMSD}(t)$ ) between the predicted and reference RMSD values at each time step ( $t$ )

$$\Delta\text{RMSD}(t) = |\text{RMSD}(t) - \text{RMSD}_{\text{Ref}}(t)|. \quad (14)$$

The reference RMSD ( $\text{RMSD}_{\text{Ref}}$ ) was obtained from Cartesian coordinates calculated from the collective variables coordinates, instead of directly from the original Cartesian coordinates, as the two have been proven consistent in our previous work.

## III. APPLICATION

We evaluated our method on two distinct systems. First, the accuracy of our tree-representation method for multi-chain proteins was assessed by reconstructing the long, multi-chain protein 3sj9. Subsequently, the universality of our Transformer-based force field was demonstrated using the single-chain protein 112y and the two-chain protein 1bom for training. These smaller proteins were chosen for force field training due to computational resource limitations, as training on the larger 3sj9 would require significantly more memory. We employ the GROMACS<sup>18–20</sup> software (version 2022.2) for the MD simulations, utilizing a timestep of 2 femtosecond (fs) and saving trajectories every 0.1 nanoseconds (ns).

### A. Multichain structure representation

In this section, we present the results of applying our reconstruction method to the 187-amino-acid, two-chain protein 3sj9<sup>21</sup> to assess its accuracy for multi-chain systems. As illustrated in Figure 2, the reconstructed structure closely aligns with the original structure. A detailed comparison reveals good agreement for both backbone and side-chain bonds. Quantitatively, the RMSD between the reconstructed and original structures is 0.28 Å for backbone atoms and 0.43 Å for all heavy atoms. These low RMSD values indicate a near-native reconstruction. Our analysis suggests that the small discrepancies observed primarily arise from minor deviations in bond lengths within the terminal amino groups.

### B. Multi-protein simulation

To evaluate the code, we used two proteins as templates: a 20-amino-acid single-chain protein, 112y<sup>22</sup>, and a 46-amino-acid two-chain protein. Molecular dynamics simulations were carried out for 100 ns for both proteins, and trajectory frames were saved at 0.1 ns intervals. The training dataset comprised four trajectories. Specifically, it included the MD trajectories of 112y and 1bom, as well as virtual trajectories representing the individual chains of 1bom. These virtual trajectories were derived from the original 1bom trajectory and were added to enhance the model’s accuracy in representing 1bom. Each trajectory consisted of 1000 structures.

Based on the analysis presented in the Methods section, the minimum tensor dimension required for representing each amino acid is 40. However, to ensure compatibility with different amino acid configurations, we use a tensor dimension of 160. An adaptive learning rate scheme is implemented, adjusting the learning rate based on the training loss. Our model employs two Transformer layers. The dense layers within  $\mathbb{D}_S$  and  $\mathbb{D}_E$  each contain a single hidden layer with 3200 units. Following our previous work, the LeakyReLU activation function is consistently used in all Transformer layers and the dense layers of  $\mathbb{D}_S$  and  $\mathbb{D}_E$ .

After training the model, we generate trajectories by iteratively applying the learned propagator,  $\mathbb{F}_0$ . We begin with

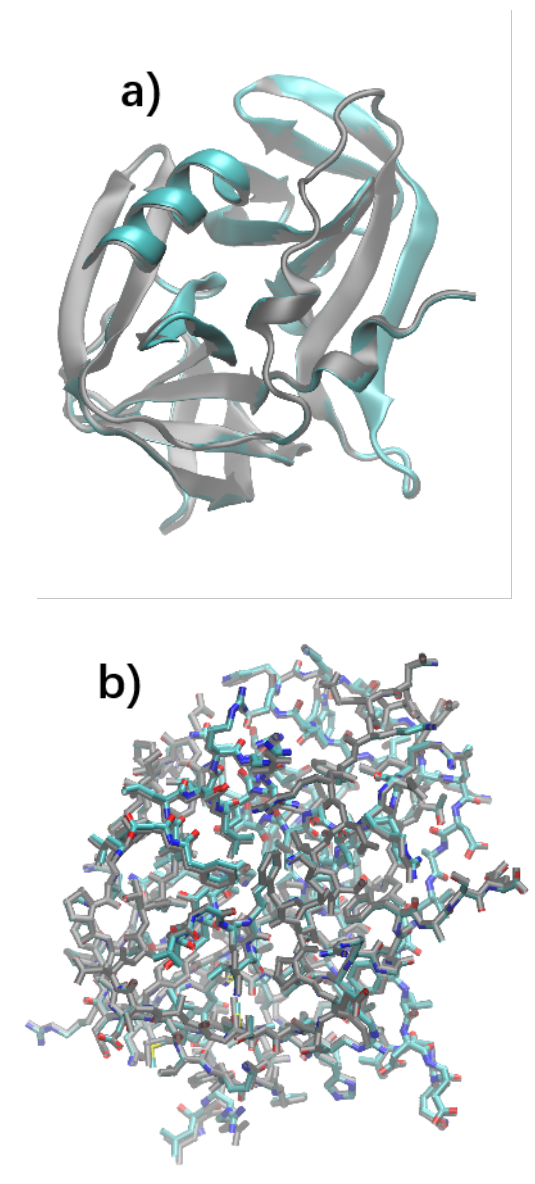


FIG. 2: The structure reconstruction of a two-chain protein 3sj9 with a) overall performance and b) bond math details.

The cyan color labels the reference structure and the gray color labels the re-constructed structure.

the first frame of the MD trajectory as the initial structure. Each subsequent frame is then generated conditioned only on the previous frame's coordinates. This generative process achieves a speedup of approximately 10,000 times relative to standard molecular dynamics computations. To assess the accuracy of the generated trajectory, we compare it to the original MD trajectory using the RMSD of the CA atoms. The RMSD of CA atoms provides a sensitive measure of structural similarity, as it is highly responsive to even small changes in individual amino acid conformation. It is important to emphasize that we use only the first frame of the MD data to initiate the generation process; all subsequent frames are de novo generated. This constitutes a stringent test, as errors in

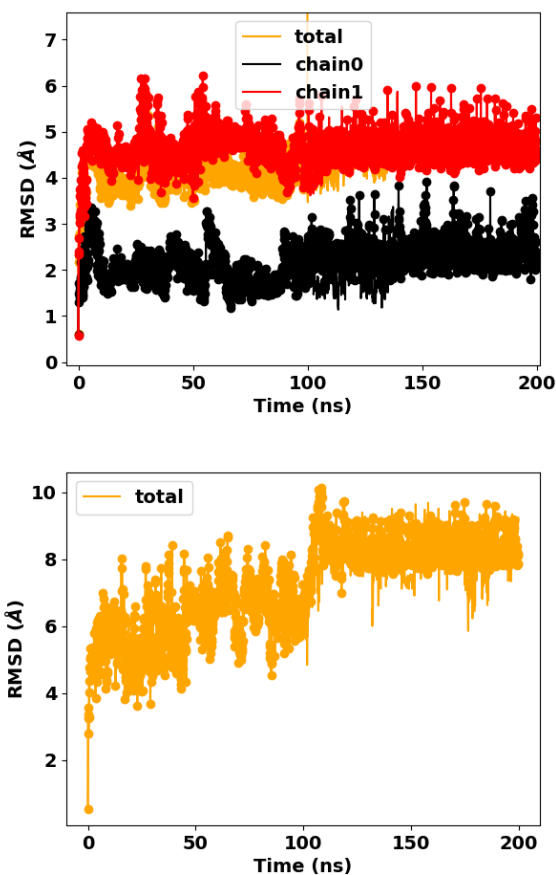


FIG. 3: RMSD profiles of molecular dynamics simulations for 1bom (top) and 112y (bottom). Orange, black, and red lines show RMSD values for the total protein, first chain, and second chain, respectively. Solid lines represent results from original MD simulations; dotted lines represent model-generated data.

propagation can accumulate, and any single incorrect step can lead to significant deviations in the generated trajectory.

The RMSD profiles for 1bom and 112y are displayed in Figure 3. The model was trained using the first 100 ns of the molecular dynamics trajectory. Within this training window, the predicted RMSD values closely match the actual values, indicating accurate interpolation of the trajectory. Extrapolating beyond the training data, the model maintains good agreement with the RMSD profiles of the individual chains of 1bom up to 200 ns, demonstrating its strong extrapolation capabilities. The RMSD of the total protein of 1bom also shows reasonable agreement with the simulation data in interpolation. The importance of including individual chain data in the training process is illustrated in Figure C.1 (Appendix), which shows reduced extrapolation accuracy beyond 100 ns when this data is omitted.

### C. Propagation with Noise

The Methods section outlines how dropout within the Transformer module can be used to introduce noise into the SDE. For 1bom, we observed that a dropout rate of 0.0001 facilitated exploration of a larger range of protein configurations (see Figure 5). While the RMSD values for the individual chains remained close to the true values, they exhibited increased oscillations, indicating exploration of a broader region of configuration space. However, when the dropout rate was increased to 0.0002, the generated trajectory for 1bom deviated substantially from the true MD trajectory, with the total RMSD becoming inaccurate even within the training data regime. In the case of 112y, both dropout rates (0.0001 and 0.0002) led to worse performance in the extrapolation region (beyond 100 ns), suggesting that a smaller noise level is necessary for this protein, see Figure 4. These results demonstrate the need for careful calibration of the dropout rate (and thus the noise level) for different protein targets. We hypothesize that with a sufficiently large and diverse MD training dataset, encompassing most of the relevant configuration space, noise can be introduced more effectively to promote exploration of even more raw states.

### IV. CONCLUSION AND OUTLOOK

This work introduces a unified Transformer-based framework for approximating molecular dynamics trajectories of multi-chain proteins. Extending a previous single-chain, tree-structured network, we demonstrate accurate reconstruction of the long protein 3sj9. We present a novel method for representing collective variables as language-like sequences, enabling the use of a Transformer-based model as a propagator for drift force. Using generated trajectories for training, we achieve a 10,000x speedup in molecular dynamics simulations. Our trained model generalizes to both interpolation and extrapolation on the 1bom and 112y protein systems, demonstrating its potential as a universal protein propagator.

While this work focuses on presenting the methodology and, due to computational limitations, demonstrates its application on only two proteins, we anticipate that with sufficient data and resources, the model can be generalized to all proteins, leading to dramatic acceleration of molecular dynamics simulations.

#### Appendix A: Example amino structure

#### Appendix B: Amino Acid hierarchy

#### Appendix C: Alternative training

<sup>1</sup>S. A. Hollingsworth and R. O. Dror, “Molecular Dynamics Simulation for All,” *Neuron* **99**, 1129–1143 (2018).

<sup>2</sup>M. I. Zimmerman and G. R. Bowman, *Methods in Enzymology*, 1st ed., Vol. 578 (Elsevier Inc., 2016) pp. 213–225.

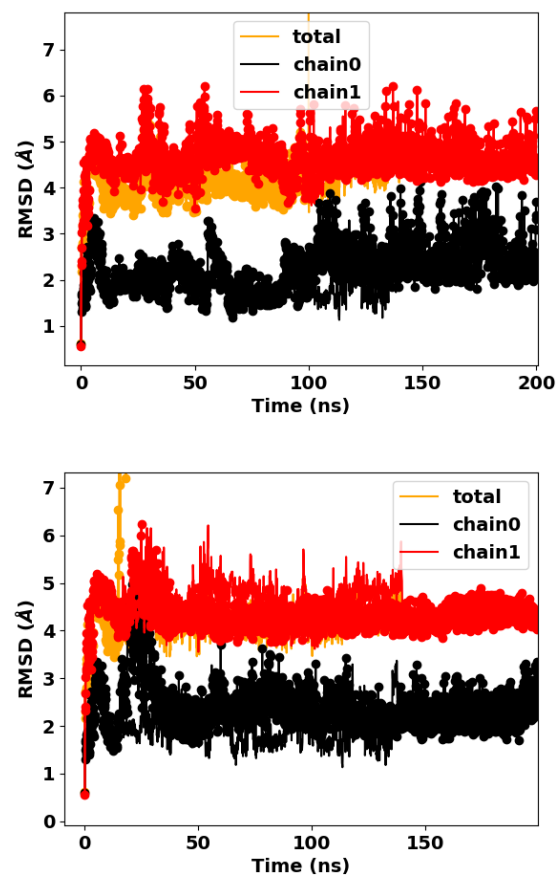


FIG. 4: RMSD profiles of molecular dynamics simulations for 1bom with dropout parameter 0.0001 (top) and 0.0002 (bottom). Orange, black, and red lines show RMSD values for the total protein, first chain, and second chain, respectively. Solid lines represent results from original MD simulations; dotted lines represent model-generated data.

<sup>3</sup>M. Bergdorf, A. Robinson-Mosher, X. Guo, K.-H. Law, D. E. Shaw, and D. E. Shaw, “Desmond/GPU Performance as of April 2021,” **1** (2021).

<sup>4</sup>D. E. Shaw, P. J. Adams, A. Azaria, J. A. Bank, B. Batson, A. Bell, M. Bergdorf, J. Bhatt, J. Adam Butts, T. Correi, R. M. Dirks, R. O. Dror, M. P. Eastwo, B. Edwards, A. Even, P. Feldmann, M. Fenn, C. H. Fenton, A. Forte, J. Gagliardo, G. Gill, M. Gorlatova, B. Greskamp, J. P. Grossman, J. Gullingsrud, A. Harper, W. Hasenplaugh, M. Heily, B. C. Heshmat, J. Hunt, D. J. Ierardi, L. Iserovich, B. L. Jackson, N. P. Johnson, M. M. Kirk, J. L. Klepeis, J. S. Kuskin, K. M. Mackenzie, R. J. Mader, R. McGowen, A. McLaughlin, M. A. Moraes, M. H. Nasr, L. J. Nociolo, L. O’Donnell, A. Parker, J. L. Peticolas, G. Pocina, C. Predescu, T. Quan, J. K. Salmon, C. Schwink, K. S. Shim, N. Siddique, J. Spengler, T. Szalay, R. Tabladillo, R. Tartler, A. G. Taube, M. Theobald, B. Towles, W. Vick, S. C. Wang, M. Wazlowski, M. J. Weingarten, J. M. Williams, and K. A. Yuh, “Anton 3: Twenty Microseconds of Molecular Dynamics Simulation before Lunch,” *International Conference for High Performance Computing, Networking, Storage and Analysis, SC*, 1–11 (2021).

<sup>5</sup>R. C. Bernardi, M. C. Melo, and K. Schulten, “Enhanced sampling techniques in molecular dynamics simulations of biological systems,” *Biochimica et Biophysica Acta - General Subjects* **1850**, 872–877 (2015).

<sup>6</sup>W. G. Noid, “Perspective: Coarse-grained models for biomolecular systems,” *Journal of Chemical Physics* **139** (2013), 10.1063/1.4818908.

<sup>7</sup>A. Liwo, C. Czaplowski, J. Pillardy, and H. A. Scheraga, “Cumulant-based

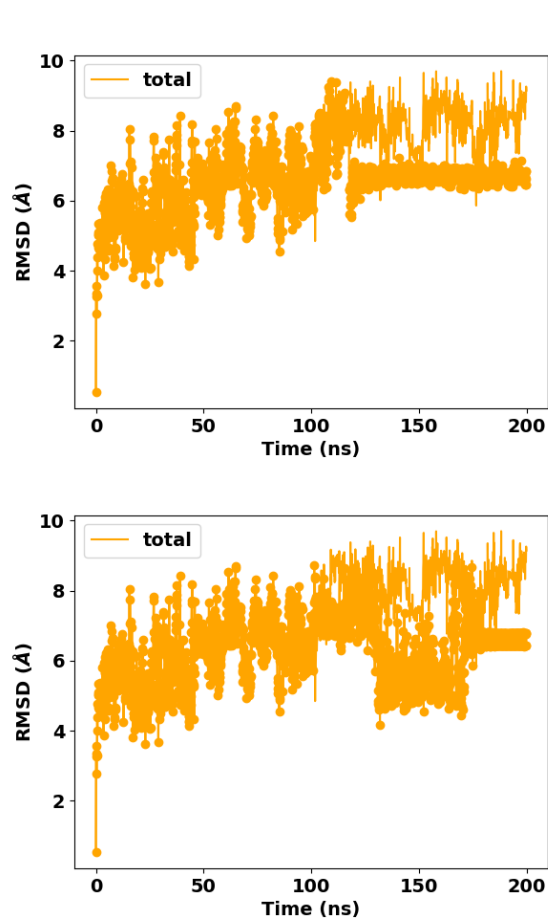


FIG. 5: RMSD profiles of molecular dynamics simulations for 112y with dropout parameter 0.0001 (top) and 0.0002 (bottom). Orange, black, and red lines show RMSD values for the total protein, first chain, and second chain, respectively. Solid lines represent results from original MD simulations; dotted lines represent model-generated data.

expressions for the multibody terms for the correlation between local and electrostatic interactions in the united-residue force field,” *Journal of Chemical Physics* **115**, 2323–2347 (2001).

<sup>8</sup>C. Mim, H. Cui, J. A. Gawronski-Salerno, A. Frost, E. Lyman, G. A. Voth, and V. M. Unger, “Structural basis of membrane bending by the N-BAR protein endophilin,” *Cell* **149**, 137–145 (2012).

<sup>9</sup>J. W. Chu and G. A. Voth, “Allostery of actin filaments: Molecular dynamics simulations and coarse-grained analysis,” *Proceedings of the National Academy of Sciences of the United States of America* **102**, 13111–13116 (2005).

<sup>10</sup>A. Yu, A. J. Pak, P. He, V. Monje-Galvan, L. Casalino, Z. Gaieb, A. C. Dommer, R. E. Amaro, and G. A. Voth, “A multiscale coarse-grained model of the SARS-CoV-2 virion,” *Biophysical Journal* **120**, 1097–1104 (2021).

<sup>11</sup>G. Tóth, “Effective potentials from complex simulations: a potential-matching algorithm and remarks on coarse-grained potentials,” *Journal of Physics: Condensed Matter* **19**, 335222 (2007).

<sup>12</sup>W. Li and S. Takada, “Characterizing protein energy landscape by self-learning multiscale simulations: Application to a designed  $\beta$ -hairpin,” *Biophysical Journal* **99**, 3029–3037 (2010).

<sup>13</sup>D. Wang, Y. Wang, J. Chang, L. Zhang, H. Wang, and W. E, “Efficient sampling of high-dimensional free energy landscapes using adaptive reinforced dynamics,” *Nature Computational Science* **2**, 20–29 (2022),

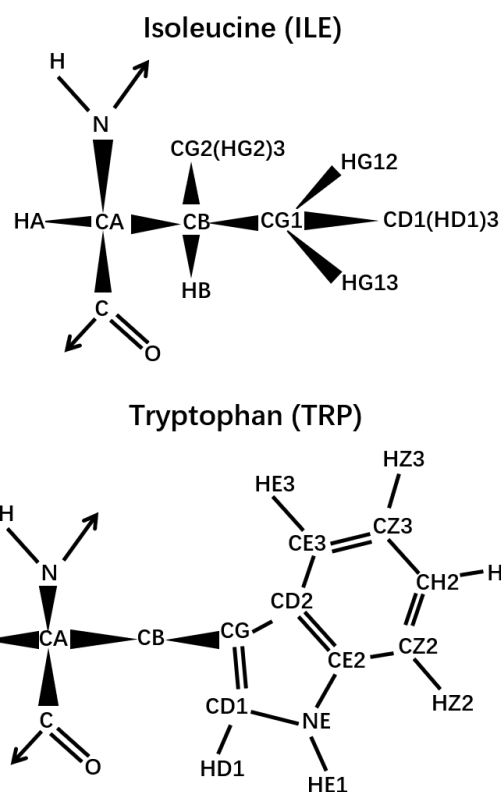


FIG. A.1: The illustration of structures of ILE (upper panel) and TRP (lower panel).

arXiv:2104.01620.

<sup>14</sup>L. Zhang, H. Wang, and E. Weinan, “Reinforced dynamics for enhanced sampling in large atomic and molecular systems,” *Journal of Chemical Physics* **148** (2018), 10.1063/1.5019675, arXiv:1712.03461.

<sup>15</sup>L. Klein, A. Y. K. Foong, T. E. Fjelde, B. Mlodozieniec, M. Brockschmidt, S. Nowozin, F. Noé, and R. Tomioka, “Timewarp: Transferable Acceleration of Molecular Dynamics by Learning Time-Coarsened Dynamics,” (2023), arXiv:2302.01170.

<sup>16</sup>J. Zhu and J. Ma, “A unified framework for coarse grained molecular dynamics of proteins,” (2024), arXiv:2403.17513.

<sup>17</sup>A. Vaswani, N. Shazeer, N. Parmar, J. Uszkoreit, L. Jones, A. N. Gomez, Ł. Kaiser, and I. Polosukhin, “Attention is all you need,” *Advances in Neural Information Processing Systems* **2017-December**, 5999–6009 (2017), arXiv:1706.03762.

<sup>18</sup>D. Van Der Spoel, E. Lindahl, B. Hess, G. Groenhof, A. E. Mark, and H. J. Berendsen, “GROMACS: Fast, flexible, and free,” *Journal of Computational Chemistry* **26**, 1701–1718 (2005).

<sup>19</sup>E. Lindahl, B. Hess, and D. van der Spoel, “GROMACS 3.0: A package for molecular simulation and trajectory analysis,” *Journal of Molecular Modeling* **7**, 306–317 (2001).

<sup>20</sup>H. J. Berendsen, D. van der Spoel, and R. van Drunen, “GROMACS: A message-passing parallel molecular dynamics implementation,” *Computer Communications* **91**, 43–56 (1995).

<sup>21</sup>G. Lu, J. Qi, Z. Chen, X. Xu, F. Gao, D. Lin, W. Qian, H. Liu, H. Jiang, J. Yan, and G. F. Gao, “Enterovirus 71 and Coxsackievirus A16 3C Proteases: Binding to Rupintrivir and Their Substrates and Anti-Hand, Foot, and Mouth Disease Virus Drug Design,” *Journal of Virology* **85**, 10319–10331 (2011).

<sup>22</sup>J. W. Neidigh, R. M. Fesinmeyer, and N. H. Andersen, “Designing a 20-residue protein,” *Nature Structural Biology* **9**, 425–430 (2002).

<sup>23</sup>J. Zhu, “Theoretical investigation of the Freeman resonance in the dissociative ionization of H<sub>2</sub><sup>+</sup>,” *Physical Review A* **103**, 013113 (2021).

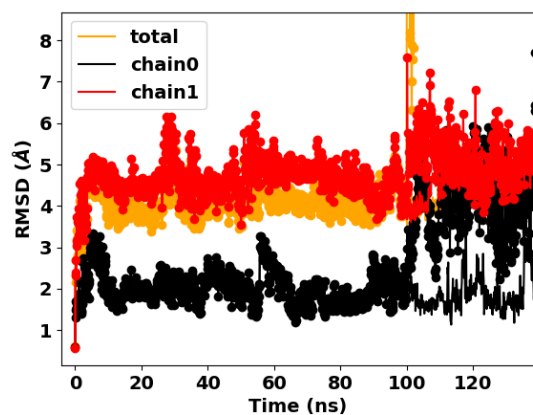


FIG. C.1: RMSD profiles of molecular dynamics simulations for 1bom, where the model is trained without single chain datas of 1bom. Orange, black, and red lines show RMSD values for the total protein, first chain, and second chain, respectively. Solid lines represent results from original MD simulations; dotted lines represent model-generated data.

- <sup>24</sup>J. Zhu and A. Scrinzi, “Electron double-emission spectra for helium atoms in intense 400-nm laser pulses,” *Physical Review A* **101**, 063407 (2020).
- <sup>25</sup>J. Zhu, “Quantum simulation of dissociative ionization of  $H_2^+$  in full dimensionality with a time-dependent surface-flux method,” *Physical Review A* **102**, 053109 (2020).
- <sup>26</sup>J. Parsons, J. B. Holmes, J. M. Rojas, J. Tsai, and C. E. M. Strauss, “Practical Conversion from Torsion Space to Cartesian Space for In Silico Protein Synthesis,” *Wiley InterScience* **0211458** (2005), 10.1002/jcc.20237.
- <sup>27</sup>G. Xu, Q. Wang, and J. Ma, “OPUS-Rota4: a gradient-based protein side-chain modeling framework assisted by deep learning-based predictors,” *Briefings in Bioinformatics* **23**, 1–10 (2022).
- <sup>28</sup>J. Jumper, R. Evans, A. Pritzel, T. Green, M. Figurnov, O. Ronneberger, K. Tunyasuvunakool, R. Bates, A. Žídek, A. Potapenko, A. Bridgland, C. Meyer, S. A. Kohl, A. J. Ballard, A. Cowie, B. Romera-Paredes, S. Nikolov, R. Jain, J. Adler, T. Back, S. Petersen, D. Reiman, E. Clancy, M. Zielinski, M. Steinegger, M. Pacholska, T. Berghammer, S. Bodenstein, D. Silver, O. Vinyals, A. W. Senior, K. Kavukcuoglu, P. Kohli, and D. Hassabis, “Highly accurate protein structure prediction with AlphaFold,” *Nature* **596**, 583–589 (2021).
- <sup>29</sup>M. K. Scherer, B. Trendelkamp-Schroer, F. Paul, G. Pérez-Hernández, M. Hoffmann, N. Plattner, C. Wehmeyer, J. H. Prinz, and F. Noé, “PyEMMA 2: A Software Package for Estimation, Validation, and Analysis of Markov Models,” *Journal of Chemical Theory and Computation* **11**, 5525–5542 (2015).
- <sup>30</sup>T. Zang, L. Yu, C. Zhang, and J. Ma, “Parallel continuous simulated tempering and its applications in large-scale molecular simulations,” *The Journal of Chemical Physics* **141**, 044113 (2014).
- <sup>31</sup>T. Zang, T. Ma, Q. Wang, and J. Ma, “Improving low-accuracy protein structures using enhanced sampling techniques,” *The Journal of chemical physics* **149** (2018), 10.1063/1.5027243.
- <sup>32</sup>C. Zhang and J. Ma, “Enhanced sampling and applications in protein folding in explicit solvent,” *The Journal of Chemical Physics* **132**, 244101 (2010), arXiv:1003.0464.
- <sup>33</sup>J. Köhler, Y. Chen, A. Krämer, C. Clementi, and F. Noé, “Flow-Matching: Efficient Coarse-Graining of Molecular Dynamics without Forces,” *Journal of Chemical Theory and Computation* **19**, 942–952 (2023), arXiv:2203.11167.
- <sup>34</sup>J. Wang, S. Olsson, C. Wehmeyer, A. Pérez, N. E. Charron, G. De Fabritiis, F. Noé, and C. Clementi, “Machine Learning of Coarse-Grained Molecular Dynamics Force Fields,” *ACS Central Science* **5**, 755–767 (2019), arXiv:1812.01736.
- <sup>35</sup>B. E. Husic, N. E. Charron, D. Lemm, J. Wang, A. Pérez, M. Majewski, A. Krämer, Y. Chen, S. Olsson, G. De Fabritiis, F. Noé, and C. Clementi, “Coarse graining molecular dynamics with graph neural networks,” *Journal of Chemical Physics* **153**, 1–16 (2020), arXiv:2007.11412.
- <sup>36</sup>J. Moulton, “A decade of CASP: Progress, bottlenecks and prognosis in protein structure prediction,” *Current Opinion in Structural Biology* **15**, 285–289 (2005).
- <sup>37</sup>J. Moulton, J. T. Pedersen, R. Judson, and K. Fidelis, “A large-scale experiment to assess protein structure prediction methods,” *Proteins: Structure, Function, and Bioinformatics* **23**, ii–iv (1995).
- <sup>38</sup>T. Ma, T. Zang, Q. Wang, and J. Ma, “Refining protein structures using enhanced sampling techniques with restraints derived from an ensemble-based model,” *Protein science : a publication of the Protein Society* **27**, 1842–1849 (2018).
- <sup>39</sup>G. Xu, Z. Luo, R. Zhou, Q. Wang, and J. Ma, “OPUS-Fold3: a gradient-based protein all-atom folding and docking framework on TensorFlow,” *Briefings in Bioinformatics* **24**, 1–8 (2023).
- <sup>40</sup>R. L. Harrison, “Introduction to Monte Carlo simulation,” *AIP Conference Proceedings* **1204**, 17–21 (2009).
- <sup>41</sup>G. Bhanot, “The Metropolis algorithm,” *Reports on Progress in Physics* **51**, 429 (1988).
- <sup>42</sup>M. Karplus and G. A. Petsko, “Molecular dynamics simulations in biology,” *Nature* **347**, 631–639 (1990).
- <sup>43</sup>G. Bussi and M. Parrinello, “Accurate sampling using Langevin dynamics,” *Physical Review E* **75**, 56707 (2007).
- <sup>44</sup>E. A. Codling, M. J. Plank, and S. Benhamou, “Random walk models in biology,” *Journal of the Royal Society Interface* **5**, 813–834 (2008).
- <sup>45</sup>T. Karmakar, A. R. Finney, M. Salvalaglio, A. O. Yazaydin, and C. Perego, “Non-Equilibrium Modeling of Concentration-Driven processes with Constant Chemical Potential Molecular Dynamics Simulations,” *Accounts of Chemical Research* **56**, 1156–1167 (2023).
- <sup>46</sup>W. Janke, “Multicanonical Monte Carlo simulations,” *Physica A: Statistical Mechanics and its Applications* **254**, 164–178 (1998).
- <sup>47</sup>H. Chen, H. Fu, C. Chipot, X. Shao, and W. Cai, “Overcoming Free-Energy Barriers with a Seamless Combination of a Biasing Force and a Collective Variable-Independent Boost Potential,” *Journal of Chemical Theory and Computation* **17**, 3886–3894 (2021).
- <sup>48</sup>A. Slavík, “Generalized differential equations: Differentiability of solutions with respect to initial conditions and parameters,” *Journal of Mathematical Analysis and Applications* **402**, 261–274 (2013).
- <sup>49</sup>Y. Song and S. Ermon, “Generative modeling by estimating gradients of the data distribution,” *Advances in Neural Information Processing Systems* **32** (2019), arXiv:1907.05600.
- <sup>50</sup>Y. Song, J. Sohl-Dickstein, D. P. Kingma, A. Kumar, S. Ermon, and B. Poole, “Score-Based Generative Modeling Through Stochastic Differential Equations,” *ICLR 2021 - 9th International Conference on Learning Representations*, 1–36 (2021), arXiv:2011.13456.
- <sup>51</sup>F. Wu and S. Z. Li, “DIFFMD: A Geometric Diffusion Model for Molecular Dynamics Simulations,” *Proceedings of the 37th AAAI Conference on Artificial Intelligence, AAAI 2023* **37**, 5321–5329 (2023), arXiv:2204.08672.
- <sup>52</sup>M. Petersen, G. Roig, and R. Covino, “DynamicsDiffusion: Generating and Rare Event Sampling of Molecular Dynamic Trajectories Using Diffusion Models,” *NeurIPS 2021 AI for Science Workshop*, 1–19 (2021).
- <sup>53</sup>J. Ho, A. Jain, and P. Abbeel, “Denosing diffusion probabilistic models,” *Advances in Neural Information Processing Systems* **2020-December**, 1–25 (2020), arXiv:2006.11239.
- <sup>54</sup>A. Nichol and P. Dhariwal, “Improved Denosing Diffusion Probabilistic Models,” in *Proceedings of Machine Learning Research*, Vol. 139 (2021) pp. 8162–8171, arXiv:2102.09672.
- <sup>55</sup>L. Dinh, J. Sohl-Dickstein, and S. Bengio, “Density estimation using real NVP,” *5th International Conference on Learning Representations, ICLR 2017 - Conference Track Proceedings* (2017), arXiv:1605.08803.
- <sup>56</sup>F. Noé, S. Olsson, J. Köhler, and H. Wu, “Boltzmann generators: Sampling equilibrium states of many-body systems with deep learning,” *Science* **365** (2019), 10.1126/science.aaw1147, arXiv:1812.01729.